Quantum state-resolved reactive scattering of F+H$_2$ in supersonic jets: Nascent HF(v,J) rovibrational distributions via IR laser direct absorption methods

William B. Chapman,[a] Brad W. Blackmon, Sergey Nizkorodov, and David J. Nesbitt[b]
JILA, University of Colorado and National Institute of Standards and Technology and Department of Chemistry and Biochemistry, University of Colorado, Boulder, Colorado 80309-0440

Supersonically cooled discharge radical atom sources are combined with high-sensitivity IR absorption methods to investigate state-to-state reactive scattering of F$+n$-H$_2\rightarrow$HF(v,J)$+$H in low-density crossed supersonic jets at center-of-mass collision energies of 2.4(6) kcal/mole. The product HF(v,J) is probed with full vibrational and rotational quantum state selectivity via direct absorption of a single mode ($\Delta\nu\approx0.0001$ cm^{-1}), tunable F-center laser in the $\Delta v=1$ fundamental manifold with near shot noise limited detection levels of 10^8 molecules/cm^3/quantum state per pulse. The high absorption sensitivity, long mean free path lengths, and low-density conditions in the intersection region permit collision-free HF(v,J) rovibrational product state distributions to be extracted for the first time. Summed over all rotational levels, the HF vibrational branching ratios are 27.0(5)%, 54.2(23)%, 18.8(32)%, and <2(2)%, respectively, into $v_{HF}=3:2:1:0$. The nascent *vibrational* distributions are in good agreement with rotationally unresolved crossed-beam studies of Neumark *et al.* [J. Chem. Phys. **82**, 3045 (1985)], as well as with full quantum close-coupled calculations of Castillo and Manolopoulos [J. Chem. Phys. **104**, 6531 (1996)] on the lowest adiabatic F+H$_2$ potential surface of Stark and Werner [J. Chem. Phys. **104**, 6515 (1996)]. At a finer level of quantum state resolution, the nascent *rotational* distributions match reasonably well with full quantum theoretical predictions, improving on the level of agreement between theory and experiment from early arrested relaxation studies. Nevertheless, significant discrepancies still exist between the fully quantum state-resolved experiment and theory, especially for the highest energetically allowed rotational levels. © *1998 American Institute of Physics.* [S0021-9606(98)00545-5]

I. INTRODUCTION

A detailed understanding of fundamental chemical reaction dynamics from first principles has represented a long-standing challenge to the chemical physics community. Although the ultimate achievement of this goal will require much further theoretical and experimental effort, there has been enormous progress in these directions in recent years. This progress largely reflects rapid advances in (i) quantum state resolved experimental techniques, (ii) development of accurate high level *ab initio* potential energy surfaces (PES), and (iii) theoretical tools for performing high-level dynamics calculations on such surfaces in full dimensionality. By virtue of the intrinsic complexity of polyatomic reaction dynamics, a logical focus of theoretical and experimental efforts has been toward fundamental three-atom hydrogen abstraction processes, the classic prototype for which has been the F+H$_2\rightarrow$HF+F reaction. Indeed, the reaction dynamics of this ''benchmark'' system has remained a central target of chemical physics research[1,2] nearly three decades

after chemiluminescence,[3–5] chemical laser,[6] and crossed-beam[7] experiments began to yield the first quantum state-to-state results.

The F+H$_2\rightarrow$HF+H chemical reaction has played an enormously important role in the development and testing of theoretical reactive scattering methods for several reasons. First of all, this system represents an excellent prototype of low-barrier exothermic H-atom abstraction, yet it is small enough in total electron number and nuclear degrees of freedom to be currently tractable with high-level *ab initio* methods. Consequently, there has been a large number of potential energy surfaces developed for this system with which to investigate the dynamics of simple atom transfer reactions.[8–12] The availability of these surfaces has facilitated detailed classical,[13–16] quasiclassical,[17–19] and quantum mechanical[20–25] studies of the reaction dynamics, in particular elucidating the final rotational, vibrational, and angular distributions of the HF(v,J) products. One major breakthrough in this direction has been the development of theoretical tools for fully converged quantum reactive scattering calculations for atom+diatom systems. In conjunction with high-quality *ab initio* methods, these combined capabilities now open up exciting prospects for a truly rigorous, ''first principles'' comparison between full quantum state-to-state resolved experiments and exact quantum reactive scattering

[a]Permanent address: New Focus, Inc., 2630 Walsh Avenue, Santa Clara, CA 95051.
[b]Author to whom correspondence should be addressed.

dynamics, at least for reactions occurring on a single adiabatic potential surface.[26–28]

The experimental literature on $F+H_2$ reactions is impressively extensive. From a thermally averaged perspective, there have been numerous temperature-dependent kinetic studies of $F+H_2$ reactions, which have provided rate constants, activation energies, and Arrhenius pre-exponential factors[29–31] for the atom abstraction event. Such results provide useful experimental constraints with which to test both potential surfaces and dynamics calculations, but the strength of these comparisons is substantially weakened by extensive thermal averaging over the initial and final quantum state distributions of reagents and products. From a more quantum state-resolved perspective, the exothermic $F+H_2$ reaction results in a strong vibrational and rotational population inversion in the HF product, which has permitted detailed studies of state-to-state reaction dynamics; for example, via tandem chemical laser gain experiments by Pimentel and co-workers.[6,32,33]

Of special historical importance have been the pioneering ''arrested relaxation'' studies of Polanyi and co-workers, which exploited FTIR chemiluminescence methods[3–5] to probe rovibrational distributions of the product $HF(v,J)$ states under low-pressure, continuous flow conditions. The key advantage of these chemiluminescence methods for H-atom abstraction is that IR emission from all rovibrational levels of the $HF(v,J)$ product can be readily resolved with modest spectral resolution. Due to finite pressures and residence times in the FTIR region, however, the newly formed HF products experienced multiple collisions and thus suffered partial rovibrational relaxation prior to detection. Consequently, the ''nascent'' (i.e., collision-free) rovibrational distributions of HF could only be estimated by repeated experiments as a function of flow cell densities and extrapolation to the zero-pressure limit. Despite limitations due to collision effects, however, the Polanyi studies provided a major advance in our understanding of A+BC reaction dynamics. Indeed, the legacy of these arrested relaxation methods has been an impressive body of state-resolved rate data for several atom+diatom systems. In turn, these data have been responsible for stimulating the development and testing of many fundamental concepts in microscopic reaction rate theory.

With even more detailed control of the reactive event, elegant crossed-molecular-beam methods developed by Lee and co-workers[7,34,35] and Toennies and co-workers[36–38] have been used to investigate *differential* reactive scattering of $F+H_2$ (and isotopic variants) for a series of center-of-mass collision energies. Under crossed-beam conditions, the number densities in the intersection region are low enough to prevent collisional relaxation of the initial $HF(v,J)$ product state distributions, which can therefore be measured by time-of-flight analysis of recoil velocities. However, even with heroic improvements in these beam techniques by Faubel *et al.*,[36–38] such time-of-flight methods still offer only rather modest kinetic energy resolution ($\approx 10^2$ cm^{-1}) of the HF product recoil in comparison with laser or chemiluminescence detection methods. As a result, these beam studies yield data primarily on HF *vibrational* populations, with

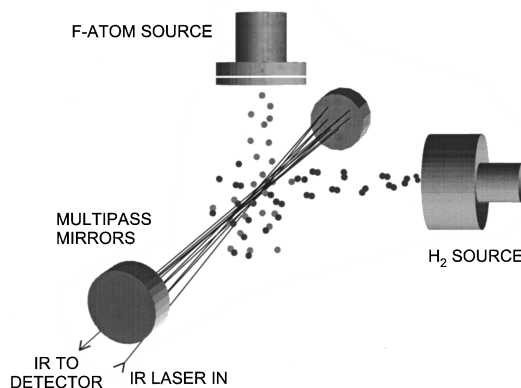## DIRECT IR LASER ABSORPTION PROBE OF REACTIVE SCATTERING IN CROSSED JETS

FIG. 1. Schematic diagram of the crossed-jet apparatus for state-to-state reactive scattering of $F+H_2 \rightarrow HF(v,J)+H$ under single collision conditions.

more limited information on rotational distributions extracted from detailed modeling and contour analysis of the time-of-flight data. Nevertheless, due to exquisite angular and center-of-mass energy resolution, these crossed-molecular-beam methods have provided the most detailed information to date on $F+H_2$ reactions, specifically on vibrational state-resolved angular distributions of reactively scattered HF. For example, the studies of Neumark *et al.*[34,35] yielded first indications of a strong dependence of differential cross sections on vibrational state, shifting from predominantly backward- to forward-scattered $HF(v)$ products for the highest energetically accessible vibrational level. These vibrationally state-resolved data stimulated considerable theoretical interest[26–28,39–41] in the possible role of dynamical quantum scattering resonances of the $F+H_2$ potential surface.

Our group has recently been developing pulsed discharge sources of jet-cooled radicals for investigation of state-to-state reaction dynamics with high spectroscopic resolution.[42,43] The sources rely on striking a discharge behind the limiting aperture of a supersonic slit or pinhole nozzle, which effectively confines the plasma in the stagnation region. In favorable systems the source can produce radical densities on the order of 10^{15}/cm^3 at the expansion orifice. These high radical densities prove sufficient for reactive scattering studies with a second jet of supersonically cooled reagents,[44] while yielding adequate product state densities for detection via shot-noise limited direct absorption with a high-resolution, tunable IR laser (see Fig. 1). The powerful advantage of such an approach is that one can simultaneously achieve *spectroscopic* (i.e., $\Delta \nu \approx 0.0001$ cm^{-1}) levels of complete product quantum state resolution, while rigorously maintaining single collision conditions. In a very interesting complementary direction, there have also been recent molecular beam measurements from Keil and co-workers[45] that combine HF chemical laser excitation and bolometric detection to probe angularly resolved, differential reactive scattering into selected rotational levels in the $HF(v=2)$ manifold.
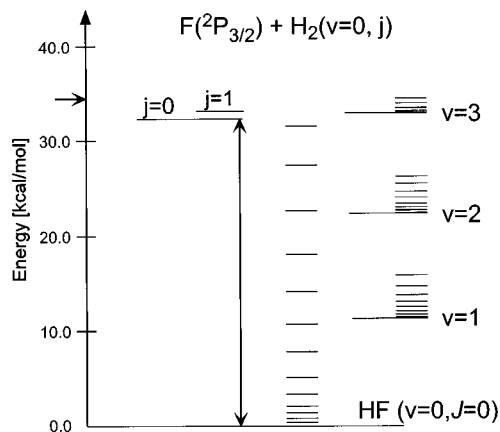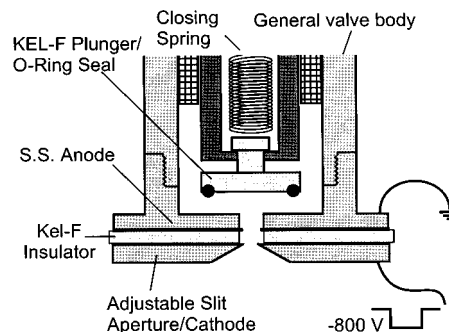
FIG. 2. Energy level diagram for $F+H_2$ reactions, demonstrating the $HF(v,J)$ product levels energetically accessible at 1.84(14) kcal/mole collision energy (1 kcal/mole=4.184 kJ/mole). The bond dissociation energies for H_2 and HF have been determined to high precision from detailed spectroscopic work, which permits the reaction exothermicity for $F(^2P_{3/2})$ $+H_2(j=0)\rightarrow HF(v=0,J=0)+H(^2S_{1/2})$ to be known to unusually high accuracy, i.e., $\Delta E=11\ 192(5)\ cm^{-1}=32.001(14)$ kcal/mole denoted by the double-sided arrow.

FIG. 3. Details of the pulsed discharge source for F-atom generation.

The focus of the present work is to exploit the high-resolution IR laser-based absorption method for extracting nascent product state distributions from the $F+H_2$ reaction under single collision conditions. Our approach is based on the following. First, a primary pulsed supersonic discharge source of F-atoms is collided with a secondary pulsed jet of H_2 molecules sufficiently far downstream of the nozzle to ensure long mean-free-path length, molecular beam collisions. Second, the H_2 beam densities and intersection path lengths are chosen to permit only a small fraction ($\lesssim3\%-4\%$) of the F-atoms to react, which for the current center-of-mass collision energy $[E_{com}=2.4(6)$ kcal/mole] and reaction exothermicity can energetically access HF products in up to $v=3$ (see Fig. 2). Third, this product $HF(v,J)$ is probed in the intersection region by high-sensitivity direct absorption of single mode tunable *F*-center laser light. As a function of laser tuning, these spectral data yield Doppler limited profiles on reactively scattered product $HF(v,J)$ over the complete manifold of vibration/rotation quantum states. Finally, in conjunction with previously measured rovibrational transition matrix elements for HF absorption/emission, nascent product state distributions can be extracted for each of the energetically accessible rovibrational levels.

The rest of this paper is organized as follows. In Sec. II, details of the experimental method are presented, followed in Sec. III by sample data and necessary experimental diagnostics. In Sec. IV we report rotationally resolved absorption/emission data for the energetically accessible $HF(v\leq3,J)$ rovibrational manifold, which are used in Sec. V to extract nascent state populations. A major focus of this work is to provide the first rigorous comparison of measured rovibrational $HF(v,J)$ populations with theoretical predictions from current state-of-the-art *ab initio*/quantum dynamics calculations. Specifically, our results are compared in Sec. VI against fully converged, three-dimensional (3-D) quantum reactive scattering calculations performed by Castillo and Manolopoulos[28] on the lowest adiabatic $F(^2P_{3/2})+H_2$ poten-

tial energy surfaces of Stark and Werner,[27] with additional comparisons made with previous experimental studies of Lee and co-workers[34,35] and Polanyi and co-workers.[4] Conclusions and directions for future work are summarized in Sec. VII.
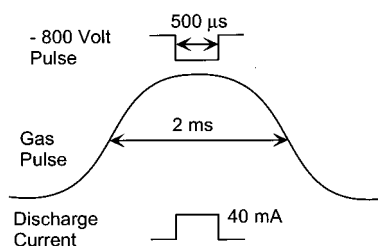
II. EXPERIMENT

The experimental apparatus for state-to-state *reactive* scattering of $F+H_2$ is based on a modification of earlier experiments for investigating state-to-state *inelastic* scattering, schematically shown in Fig. 1. The main technical advance that makes these reactive scattering experiments possible has been the development of pulsed slit discharge sources to produce high densities/absorption path lengths of jet-cooled radicals.[43,44] The success of these techniques for high-resolution, jet-cooled radical spectroscopy has prompted us to further develop smaller pinhole and/or mini-slit apertures for use in reactive scattering experiments, as elucidated in Fig. 3. Basically, a thin (~0.5 mm) discharge region is formed by gated voltage pulses ($\approx300-1000$ V) applied across a Vespel insulator between the valve body and shaped electrodes that form the limiting expansion aperture. This design fully localizes the discharge behind the nozzle orifice, which therefore permits efficient jet cooling of the expanded radical species down to $T_{rot}\approx10-20$ K. Furthermore, the thickness of the discharge region limits the residence time of the precursor radical species in the discharge to $\lesssim1\ \mu s$, which effectively eliminates subsequent bimolecular or termolecular radical chemistry from taking place. As noted in previous work,[43,44] it is also important that the voltage pulse polarity across the electrode/aperture be *negative* with respect to the valve body, which allows the heavier cations to flow *downstream* while permitting higher mobility electrons

to flow *upstream* against the bulk gas flow. This promotes a much more stable, volume-filling glow discharge instead of spatially localized filamentary breakdown.

The pulsed discharge generates on the order of 10^{15} F-atoms/cm^3 upstream of the limiting expansion orifice. The stagnation gas for the current studies is 5% F_2 in He at 50–100 Torr (1 Torr=133.3 Pascal), though other F-atom precursors such as CF_4 and SF_6 have also been investigated. The discharge strikes automatically by applying ≈ -800 V bias to the electrode/aperture during the ≈ 1–2 ms gas pulse. Computer-controlled timing circuits limit the discharge to a short temporal window (≈ 500–700 μs) near the peak of the gas flow. This serves both to better match the timing of the H_2 pulse and to eliminate occasional arcing in the vacuum chamber between pulses. The resulting 10–40 mA peak currents are stabilized with a ballast resistor (1–5 kΩ) in series with the discharge. The F-atoms are presumably formed from F_2 in the stagnation region by rapid associative detachment[46] occurring at near Langevin rates ($k_L \approx 10^{-7}$ cm^3/mol^{-1}/s^{-1}),

$$F_2 + e^- \rightarrow F + F^-, \tag{1}$$
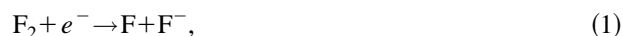
energetically driven by the electron affinity of F.[47]

Both slit and pinhole modifications of the source have been used for F-atom generation. Because the small slit source (300 μm×5 mm) is used at an order of magnitude longer distance (≈ 4.5 cm) from the probe volume than the slit length, the F-atom density in the beam intersection region is effectively similar to a pinhole orifice of the same cross-sectional area. Indeed, relative HF(v,J) populations measured with the two source geometries are identical within experimental uncertainty, and thus the choice between pinhole and small slit aperture sources is largely a matter of convenience. However, long-term stability of the discharge is empirically found to be much better with the slit source, providing over 100 h of operation between routine maintenance. With pulsed valve repetition rates kept to $\leqslant 10$ Hz, a 10 inch diffusion pump equipped with a liquid N_2-cooled baffle maintains a background pressure of $\leqslant 5 \times 10^{-5}$ Torr in the 64 L vacuum chamber.

The H_2 supersonic jet is formed through a piezoelectric valve based on the design of Proch and Trickl.[48] The conditions are 100–400 Torr backing pressure of neat H_2 or H_2/rare gas mixtures with a typical pulse duration of 300 μs and effective aperture diameter of 200 μm. The H_2 stretch is IR inactive, thus it is not possible to probe the rotational distribution of the jet-cooled H_2 reagent beam with direct absorption laser methods. Alternatively, however, dopant levels of IR absorbing molecules with comparable energy spacings are used as a rotational ''thermometer'', based on collisional equilibration in the expansion. Specifically, the jet rotational temperatures have been independently characterized in separate experiments by adding 1% CH_4 to the stagnation mixtures, and monitoring direct IR absorption out of individual rotational levels in the ν_3 CH stretch absorption band.[49] For typical stagnation pressures and expansion conditions, the CH_4 is almost completely cooled down into the lowest $A(J=0)$, $F(J=1)$ and $E(J=2)$ levels allowed by nuclear spin symmetry. From a Boltzmann analysis, the ro-

tational temperature is found to be on the order of $T_{rot} \approx 30$ K, which provides a lower limit for the H_2 distributions. However, even if cooled only to $T_{rot} \approx 100$ K, H_2 would still be essentially collapsed into its lowest nuclear spin-allowed states, namely $j=1$ (ortho) and $j=0$ (para) in a 3:1 ratio, with the first excited para ($j=2$) and ortho ($j=3$) state populations down by an additional 2–3 orders of magnitude.

The crossed jets intersect 4.5 cm downstream of the nozzles, where for typical backing pressures and peak gas densities in the intersection region, the F-atoms have $\leqslant 3$%–4% probability of colliding and reacting with H_2. This is comparable to the probability of subsequent inelastic collisions of the resulting HF(v,J) products in the reaction zone; any rovibrational relaxation of the HF(v,J) distributions is therefore also limited to a few percent even for gas kinetic processes, which is explicitly verified in Sec. IV by stagnation pressure-dependent studies as a function of beam density. The time profile of both F-atom and H_2 gas pulses is monitored with miniature hearing aid microphones mounted inside the vacuum chamber on translatable stages, which facilitates temporal overlap of gas pulses in the intersection region.

III. SAMPLE DATA AND DIAGNOSTICS

The HF(v,J) reaction products are probed on $\Delta v = 1$, P or R branch transitions with a single-mode, color-center laser beam multipassed 16 times through the intersection region with a cylindrical Herriot cell.[50] Near shot-noise limited absorption sensitivities are achieved by a combination of (i) dual beam differential detection on matched InSb detectors and (ii) electro-optic servo control of the color-center laser intensity, with feedback from IR light on a reference detector used to correct the intensity of the Kr$^+$ pump laser. This servo-loop control permits readily detectable signals at $\leqslant 10^{-5}$ absorbance levels in a 10 KHz detection bandwidth, which for ≈ 500 MHz Doppler-broadened lines of HF translates into sensitivities on the order of $\leqslant 10^8$ mol/cm^3/quantum state per pulse. The laser wavelengths of specific HF rovibrational transitions[51,52] are located to within their Doppler widths using a traveling Michelson interferometer of the Hall and Lee design.[53] Sample time domain absorption data is shown in Fig. 4, where the laser is tuned to the top of the Doppler profile for the $R(1)$ line of the $v=4 \leftarrow 3$ vibrational manifold and signal averaged for ≈ 1000 pulses. The F-atom discharge voltage is ≈ 500–700 μs long and centered on the H_2 pulse; thus, the nascent HF absorption signal directly maps out the 300 μs profile of the H_2 gas flow. The signals correspond to peak absorbances of ≈ 0.14% and an rms absorbance noise floor of $\approx 7 \times 10^{-6}$.

It is worth noting that direct IR laser absorption techniques naturally yield absorbance signals in *absolute* units; in conjunction with known IR transition moments, this permits the *absolute* column integrated concentrations (or more rigorously concentration *differences*) of HF(v,J) to be determined directly. For example, the peak HF absorbance signal in Fig. 4 corresponds to an absolute column integrated den-
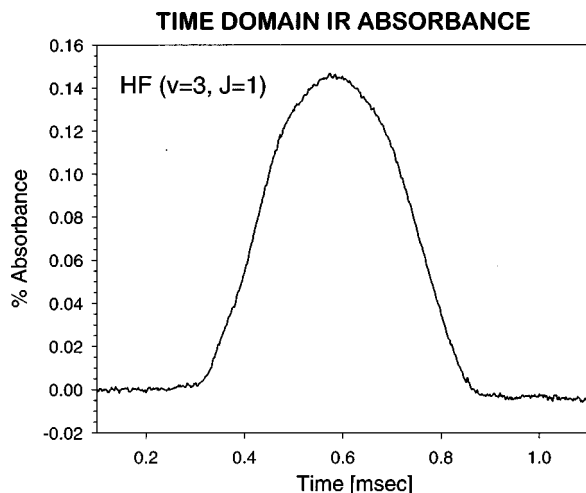
TIME DOMAIN IR ABSORBANCE

FIG. 4. Time domain signals for HF($v=3,J=1$) generated from F+H$_2$ reactions in the crossed jets, demonstrating the high signal-to-noise levels achievable in the apparatus. These signals are obtained by direct absorption of an amplitude-stabilized F-center laser tuned to the Doppler maximum of $R(1)$ and signal averaged for 1000 pulses. The maximum absorbance is 0.14%, with an rms noise floor of $\approx 7 \times 10^{-6}$ absorption units, corresponding to a minimum detectable HF product density $\leq 10^7$ mol/cm^3/quantum state.

sity of 2.0×10^{10} mol/cm^2, which from Doppler measurements of jet divergence translates into a quantum state-resolved product density of $[HF(v=3,J=1)] \approx 3 \times 10^9$ mol/cm^3 in the intersection region.[51–54] Based on the observed signal-to-noise ratio (S/N), this corresponds to a
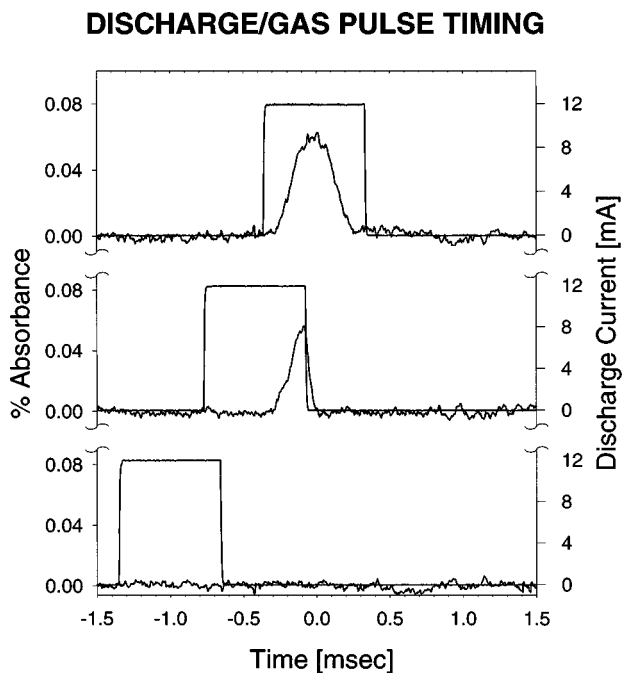
DISCHARGE/GAS PULSE TIMING

FIG. 5. Demonstration of temporal overlap between F-atom discharge with HF absorption signals. The rectangular curves represent the F-atom discharge current (scale on right), which have been progressively delayed with respect to the H$_2$ pulse centered at $t=0$. Note that the HF signals (scale on left) only occur during the precise overlap of the F-atom and H$_2$ pulses, and that the HF signals rapidly go to zero when the F-atom discharge source is shut off.
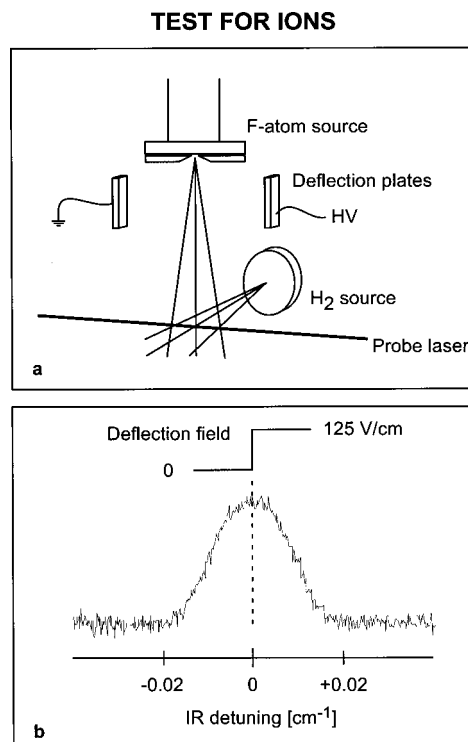
TEST FOR IONS

FIG. 6. Voltage deflection studies in order to test for possible HF formation from ions formed in the discharge. The deflection voltages have been turned on in the middle of the Doppler scan through an HF transition, with no detectable effect on the observed absorption line profiles.

minimum detection level of $[HF(v,J)]$ of $\leq 10^7$ mol/cm^3 per quantum state with only modest signal averaging.

By delaying the discharge voltage, these time domain studies also provide a simple test that HF product is formed only during the temporal overlap between F-atom and H$_2$ pulses. This is shown in Fig. 5, which displays the time-resolved HF absorption profile (centered at $t=0$) for $v=4 \leftarrow 3$, $R(1)$, with the discharge pulse (i) coincident with, (ii) partially overlapping, and (iii) prior to the H$_2$ pulse. The data illustrate that the HF signals faithfully map out the H$_2$ density, and for partially overlapping F-atom and H$_2$ pulses (see middle panel of Fig. 5), the HF absorption signals decay rapidly to zero when the discharge voltage is shut off. This time decay of the HF signals is consistent with the angular spread of the F-atom and H$_2$ jets, which causes some dispersion in time-of-flight delay from the nozzle orifice to the intersection region.

Although previous direct absorption studies indicate that ion densities in the intersection region are down from radical densities by at least 2 orders of magnitude,[43,44] it is nevertheless important to test explicitly for contribution of any charged species to the reactive scattering signals. To achieve this, deflector plates (2.0×4.0 cm) placed 8.0 cm apart, 0.5 cm downstream of the discharge aperture (see Fig. 6) are charged up to a 1000 V potential difference, with the deflection voltage switched on as the laser is tuned through the center frequency. The corresponding field strengths (up to 125 V/cm) are at least an order of magnitude greater than necessary to deflect charged species away from the jet intersection region. As shown clearly in Fig. 6, neither the inten-

sity nor symmetry of the absorption profile is altered by the presence of the electric deflection field, confirming negligible contributions to the observed reactive scattering signals from ion–molecule processes.

For comparison with previous theoretical and experimental studies, the center-of-mass collision energy (E_{com}) is specified in two ways. First, IR chromophores (typically CH_4) are doped at 1% levels into the two beams and used to characterize both the jet velocities and velocity distributions by high-resolution IR laser Dopplerimetry.[49,55] However, one can also measure the lab-frame speeds *in situ* for each of the gas mixtures by translating a miniature hearing aid microphone along the jet axis and measuring the time-of-flight delay in the pulse arrival. This much simpler alternative proves to be remarkably reliable, yielding centerline jet speeds accurate to within a few percent, as quantitatively confirmed both by the high-resolution Dopplerimetry studies and detailed thermodynamic calculations of an adiabatic expansion.[56,57] The angular profiles of the free jets are also independently determined via deconvolution of high-resolution Doppler profiles in each of the expansions. These center line speeds and angular distributions are then used in Monte Carlo simulations of the jet intersection region to evaluate the *mean* value and *spread* in center-of-mass collision energy, (i.e., E_{com} and ΔE_{com}), averaged over all relevant collision geometries. This proves to be especially crucial for energy-dependent studies of the quantum state-to-state $F+H_2$ reaction cross section, as reported elsewhere in detail.[57] For the present studies, however, we are interested predominantly in nascent state distributions of HF(v,J) at a single center-of-mass collision energy for neat ($\geq 99.99\%$) H_2 and 5.00% F_2/He. These measurements yield jet speeds of $2.50(8)\times10^5$ and $1.48(7)\times10^5$ cm/s, respectively, which for the current right angle collision geometry corresponds to center-line collision energies of 1.84 kcal/mole. When Monte Carlo averaged over the angular spreads determined from high resolution IR Dopplerimetry for the two jets, this translates into an average center-of-mass collision energy of 2.4(6) kcal/mole. Though somewhat larger, this is comparable to the 1.84 kcal/mole center-of-mass collision energies used by Lee and co-workers,[34,35] as well as in theoretical calculations by Manolopoulos and co-workers,[26,28,58] which prompts us to make comparison with these previous studies.

IV. RESULTS AND ANALYSIS

For each rotationally resolved transition, the time-resolved HF signals are captured by a transient digitizer, integrated over the central 100 μs portion of the pulse duration, and stored on computer as a function of laser detuning. Sample results for J-dependent absorption signals in the HF(v=3,J) manifold are shown in Fig. 7(a), obtained for single gas pulses with no signal averaging. Note the strong rotational-state dependence of the signals, which drop rapidly to zero near the energetic upper limit of HF(v=3,J=5). This provides additional confirmation that the HF is produced solely by neutral $F+H_2$ reactions and not influenced by any secondary reactions of $H+F_2$, which can energetically form[54] up to v=10. The spectral line widths ($\Delta\nu \approx 500$ MHz) are more than 2 orders of magnitude larger than
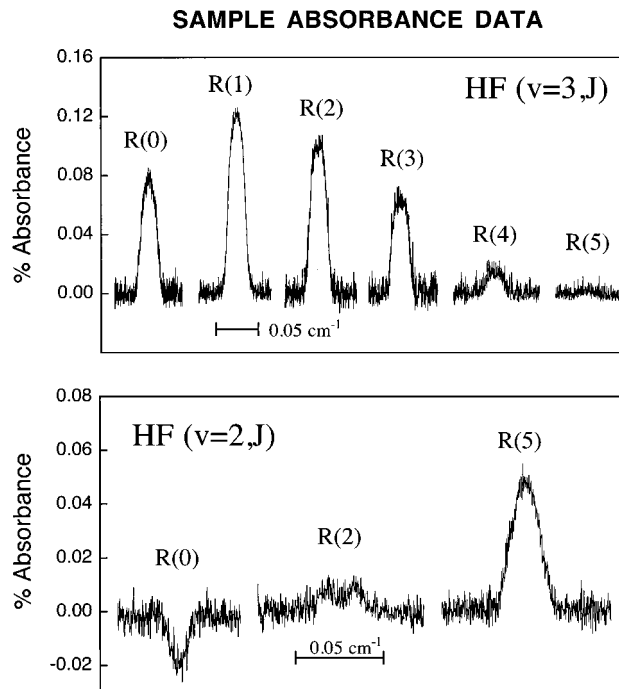

SAMPLE ABSORBANCE DATA

FIG. 7. Sample absorption data on (a) the HF(v=3,J) rotational manifold and (b) selected J-levels in the HF(v=2,J) rotational manifold, indicating full resolution of the product high-resolution Doppler line shapes. Only a single pulse is accumulated for each Doppler detuning, which accounts for the 30-fold-lower signal-to-noise ratio than observed in Fig. 4, where 1000 pulses have been averaged. Note the presence of both stimulated absorption (upper panel) and stimulated emission (lower panel) signals, depending on whether the reaction leads to a population inversion on the transition of interest. Note also that the profiles show definite Doppler structure (lower panel) at high and low detuning, which reflects information on velocity distributions of the nascent HF(v,J) products.

the laser line width ($\Delta\nu \approx 1$ MHz), thus demonstrating velocity-resolved Doppler profiles for the reactively scattered HF(v,J) product. In principle, these Doppler profiles can be analyzed to extract perpendicular velocity distributions in the lab frame for quantum state-resolved HF products. However, there are significant contributions to these linewidths due to angular divergence of the jets; thus, a detailed Doppler analysis of the recoil velocities is deferred until data in a skimmed expansion geometry is available. For present purposes, the signals are integrated over the observed Doppler profiles, which rigorously yield absolute column-integrated densities over the absorption path length.

Formation of product HF(v=4,J=0) is significantly endothermic (≈ 8 kcal/mole) and therefore energetically inaccessible at 1.84(14) kcal/mole center-of-mass collision energies. Thus, the v=4$\leftarrow$3 signals in Fig. 7(a) reflect pure absorbance due to optical excitation out of the HF(v=3,J) manifold. However, direct absorption methods coherently probe the *competition* between stimulated absorption and emission phenomena; hence, the HF(v,J) signals reflect degeneracy weighted population *differences* between the upper and lower rovibrational states. This is especially relevant for strongly exothermic processes such as $F+H_2$ that populate a large manifold of vibrational levels. Figure 7(b) illustrates one such set of data obtained from v=3$\leftarrow$2 transitions out of the v=2 vibrational manifold, which for sufficiently low
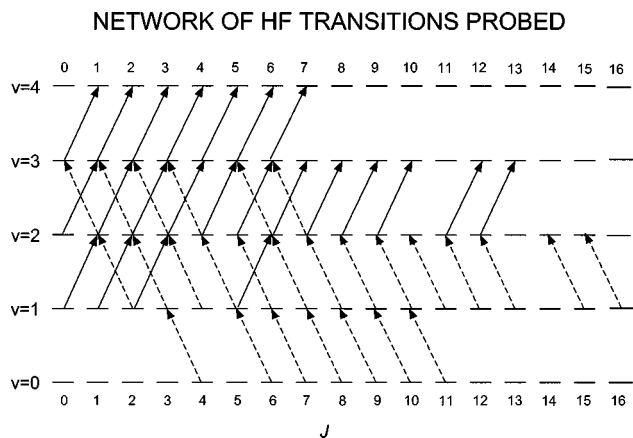
NETWORK OF HF TRANSITIONS PROBED

FIG. 8. Network of absorption transitions probed in HF(v,J) product from F+H$_2$ reactions, which permits quantitative mapping-out populations in v = 3, 2, 1 and 0 vibrational levels as a function of rotational J-state.

J-values access upper $v = 3$ states directly populated by the F+H$_2$ reaction. Thus, more generally speaking, the observed signals reflect the lower (v,J) and upper (v',J') state populations according to[54]

$$\int A(\nu)d\nu = \frac{8\pi^3\nu}{3hc}|\mu_{v'v}(m)|^2|m(J)|\left(\frac{[\mathrm{HF}(v,J)]}{2J+1}\right.$$
$$\left. -\frac{[\mathrm{HF}(v',J')]}{2J'+1}\right)\cdot l, \qquad (2)$$

where $\int A(\nu)d\nu$ is the integrated absorbance for a single rovibrational transition (unprimed/primed quantities refer to the lower/upper vibrational manifold); $\mu_{v',v}(m)$ is the transition dipole moment; and $m(J) = -J$ or $J+1$ for *P*- or *R*-branch transitions, respectively. The signals can therefore appear as net stimulated absorption or emission (i.e., ''negative absorption'') depending upon the sign of the degeneracy weighted population differences.

By way of example, the first profile in Fig. 7(b) is a scan over the $v = 3 \leftarrow 2 R(0)$ transition which near line center appears as stimulated *emission*, indicating that for slow HF products the degeneracy weighted population of HF($v = 3,J = 1$) *exceeds* that of HF($v = 2, J = 0$). However, the population inversion changes sign symmetrically in the wings of the Doppler profile, consistent with the greater HF velocity recoil anticipated for comparable J-levels in the $v = 2$ vs 3 manifold. For $v = 3 \leftarrow 2, R(2)$, both upper and lower populations are large, but the measured population *difference* is small and integrates to a net absorption. Again, the Doppler structure reveals subtle velocity structure in the degeneracy weighted population differences. Specifically, the signal becomes slightly more *positive* in the high-velocity wings of the Doppler profile. The third transition is $v = 3 \leftarrow 2, R(5)$ and appears as a pure absorption due to the absence of significant population in HF($v = 3, J = 6$).

To extract nascent HF product distributions, we first obtain an overdetermined set of integrated absorption signals that interconnect rovibrational levels in the energetically accessible manifold (see Fig. 8). The necessary dipole matrix moments and frequencies for each fully rovibrationally specified HF transition are known from previous work by

Aruman *et al.*[54] and Ram *et al.*[51] Analysis of this data can proceed in one of two ways. First, since $v = 3$ is the highest vibrational state populated by the reaction, the $v = 4 \leftarrow 3$ integrated absorption measurements probe the HF($v = 3,J$) populations directly, which can be independently fit without reference to any lower vibrational manifold. Next, the HF($v = 2,J$) distributions can be extracted from least-squares fits to the $v = 3 \leftarrow 2$ data alone, where the $v = 3$ populations are taken from the above least-squares fit. This procedure can then be repeated for each successive vibrational manifold, yielding rovibrationally resolved data on $v = 3, 2, 1$, and 0. It is worth noting that this study reflects the first rotationally resolved product detection in the *vibrationless* HF($v = 0,J$) channels, which underscores one unique advantage of IR absorption vs emission-based probe methods.

A corresponding disadvantage is that absorption methods tend to amplify experimental uncertainties for the lower vibrational levels, since these depend on uncertainties in the progressively higher vibrational levels. Specifically, all other noise contributions being the same, one can easily show that the uncertainty grows with the square root of vibrational steps away from the highest populated level. To help minimize these effects, the input data represent an average over multiple spectroscopic measurements for each transition, with as many as 80 separate experimental measurements on a given vibrational manifold taken over the course of several months. From these studies, the populations in HF($v = 0,J$) are found to be zero within experimental uncertainty for each of several rotational levels tested (i.e., $J = 4-11$). This is in good agreement with the rotationally unresolved beam data of Neumark *et al.*[34,35] as well as theoretical predictions[58] on the Stark and Werner surface.[27]

Alternatively, we have combined a least-squares fit to the entire set of integrated absorbance data. Since we do not have data on the HF($v = 0,J$) manifold for all energetically accessible J-values, the populations for $v = 0$ are fixed at zero, consistent with the above analysis. This does not eliminate the issue described above of propagating uncertainties, since populations for the higher vibrational levels will be successively less correlated with the lower vibrational manifolds and therefore better determined. Nevertheless, this method is somewhat more reliable, since it permits a physically appropriate weighting of data by number of measurements and propagation of errors throughout the rovibrational manifold. The results for all HF(v,J) states populated by the F+H$_2$ reaction are listed in Table I and plotted in Fig. 9, where the total population summed over all J-levels is set equal to 100%.

Since the HF product spends only a few μs in the laser probe region, any change in nascent population due to spontaneous emission is completely negligible (i.e., <0.1%). More potentially significant are effects due to the probe laser itself, which can in principle modify the nascent populations by stimulated emission processes. This is especially important under collision-free conditions, where the homogeneous absorption cross sections are limited predominantly by transit time broadening and can be much larger than the peak cross sections under pressure-broadened conditions. However, by limiting the power of the probe laser to below 50

TABLE I. Nascent HF(v,J) populations (in percent) from F+n-H$_2$ reactive collisions at E_{com}=1.84(14) kcal/mole. The analysis indicates the HF(v=0) populations summed over all J to be <2% and are not included in the final least-squares fits (see text for details).

J	Nascent HF(v,J) populations (%)		
	$v=3$	$v=2$	$v=1$
0	2.59 (09)	1.43 (09)	0.40 (24)
1	6.72 (06)	3.72 (20)	0.98 (46)
2	7.76 (15)	5.20 (17)	1.39 (56)
3	5.49 (17)	6.12 (30)	1.76 (49)
4	2.84 (19)	6.90 (26)	2.26 (65)
5	1.23 (15)	7.60 (32)	1.81 (43)
6	0.34 (36)	7.05 (20)	2.44 (40)
7		5.48 (43)	2.02 (36)
8		4.31 (27)	1.46 (52)
9		2.80 (49)	1.42 (50)
10		1.84 (150)	0.81 (58)
11		1.22 (93)	0.40 (170)
12		0.54 (120)	0.22 (110)
13			0.35 (150)
14			0.32 (100)
15			0.53 (48)
16			0.26 (38)

μW, this contribution is less than a few percent, which is considerably smaller than the quoted experimental uncertainties.

As a final note in this section, the densities in the intersection region are kept intentionally low to prevent any collisional relaxation of the nascent HF(v,J) distribution. This can be explicitly tested by measuring rotational branching ratios into low and high J-states as a function of reagent H$_2$ density. In the single collision limit, such ratios should, of course, be independent of [H$_2$], whereas if collisional relaxation were occurring, one would anticipate an [H$_2$]-dependent shift in rotational distributions from higher to lower J-values. Figure 10 displays the ratio of integrated absorbances for $v=3\leftarrow 2R(J)$ branch transitions out of "low" ($J=2$) and "high" ($J=8$) rotational states, over a range of stagnation pressures that extends up to nearly three times the H$_2$ densities used for obtaining the HF(v,J) distributions reported in this work. Within experimental uncertainty, these ratios are independent of H$_2$ pressure, providing experimental confirmation that rotational relaxation in the intersection region is indeed negligible.

V. DENSITY-TO-FLUX TRANSFORMATION

When integrated over high resolution Doppler profiles, the direct absorption/stimulated emission signals yield absolute column integrated *densities* of the HF products in the intersection region. However, for comparison with theoretical calculations, the state-to-state reactive cross sections are most usefully defined in terms of reactively scattered *fluxes*. In order to implement rigorous comparisons with theoretical cross sections or previous beam data, one must therefore consider the density-to-flux transformation, in effect accounting for the residence time of the IR chromophore in the probe region.[55] This residence time is inversely proportional to the component of the lab-frame HF velocity perpendicular
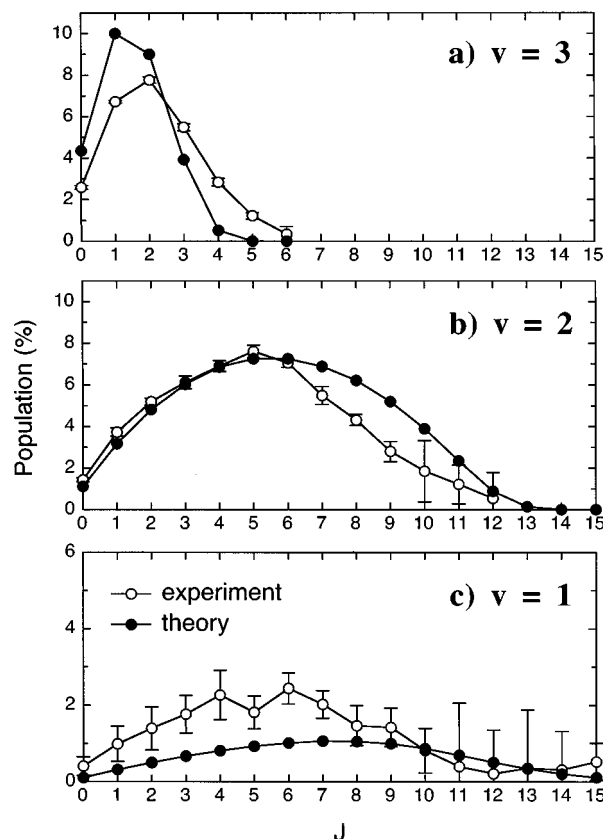

NASCENT HF(v,J) DISTRIBUTION

FIG. 9. Nascent-state product distributions (open circles) for HF(v,J) formed from F+H$_2$ reactions at E_{com}=2.4(6) kcal/mole, extracted from absorption/emission signals obtained over the network of transitions listed in Fig. 8. Signals are all scaled to sum to 100% and statistical error bars are denoted for each transition. For comparison, full quantum theoretical calculations by Castillo and Manolopoulos[58] on the SW potential surface[27] are shown in black. Note the generally good qualitative agreement with theory, though significant discrepancies are evident, most notably in the $v=3$ manifold.
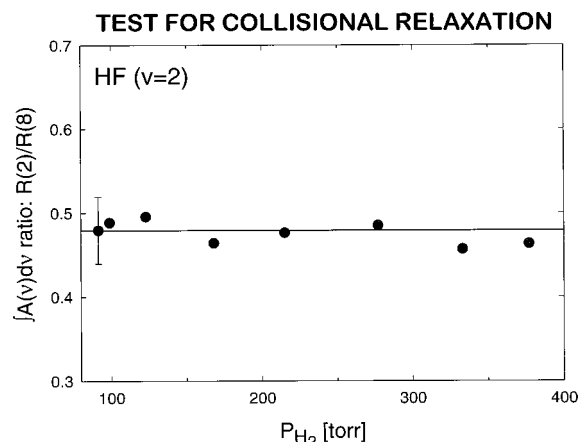

TEST FOR COLLISIONAL RELAXATION

FIG. 10. Pressure-dependent tests of integrated HF($v=2$) signal ratios (for $J=2$ and $J=8$) as a function of H$_2$ stagnation pressure density, confirming the absence of collisional relaxation of the HF(v,J) nascent distributions over a fourfold range in backing pressure and H$_2$ beam densities.

to the probe laser, i.e., $\mathbf{v}_\perp$, which in turn depends upon the product's final state and scattering angle. Although this transformation can in principle be achieved by detailed analysis of the Doppler profiles, the F+H$_2$ scattering system offers several dynamical simplifications that make this unnecessary.

First, conservation of energy and linear momentum dictates that most of the recoil energy is carried off by the light H-atom. Specifically, only $m_H/(m_H+m_{HF})\approx 5\%$ of the total recoil velocity appears in the HF. Second, as a result of such limited HF product recoil, $\mathbf{v}_\perp$ is nearly equal to the lab-frame center-of-mass velocity, making the dispersion in $\mathbf{v}_\perp$ also small. Finally, from detailed Monte Carlo simulations for the experimental geometry, any residual effect of HF recoil velocity upon these measurements is preferentially suppressed for *backward*-scattered products. Since previous differential cross section measurements of vibrationally resolved F+H$_2$ reactive scattering[34] show clearly that HF($v<3$) products are predominantly backward scattered, this further limits any influence of recoil velocity on the observed signals. There is strong forward scattering of HF into the highest vibrational level, $v=3$; however, these HF($v=3,J$) rotational states have less overall excess kinetic energy to distribute into HF product recoil, which compensates for this small effect. Thus, the density-to-flux transformation for the current scattering geometry of F+H$_2$ is expected to be largely insensitive to quantum state.

This important point can be quantitatively justified as follows. For a given product state, collision energy and center-of-mass scattering angle θ, the range of possible final lab-frame velocities depends on the azimuthal angle ϕ, about which the scattering is symmetric. For a given HF(v,J), this can be calculated from conservation of energy and numerically integrated over ϕ. In Fig. 11(a), the resulting $v_\perp(\theta)$ speeds are shown vs θ for several representative HF(v,J) product states for a perpendicular collision geometry. Note that even for the most extreme cases, the range of $v_\perp(\theta)$ varies with HF(v,J) by only $\pm 10\%$. Also, for all final states, $v_\perp(\theta)$ is nearly constant for $\theta\gtrsim\pi/2$, indicating that differential cross sections dominated by backward scattering will result in only very small corrections to perpendicular speeds in the data analysis. To take this one step further, one can use the v,J-specific differential cross sections calculated theoretically by Castillo and Manolopoulos,[58] on the Stark and Werner potential[27] to integrate $v_\perp(\theta)$ over θ for each of the final HF(v,J) states. The results are shown in Fig. 11(b) and indicate that the perpendicular speeds are predicted to be constant to within 5% for all HF(v,J) product states. Thus, to well within the reported experimental uncertainties, the fractional quantum state-resolved product *densities* shown in Table II also reflect the quantum state-resolved *fluxes*, which can therefore be directly compared with full close-coupling theoretical results in the following section.

VI. DISCUSSION

The highest level theoretical studies done to date on the F+H$_2$(j) system have been the quantum reactive scattering calculations performed by Castillo *et al.*,[28] which predict dif-
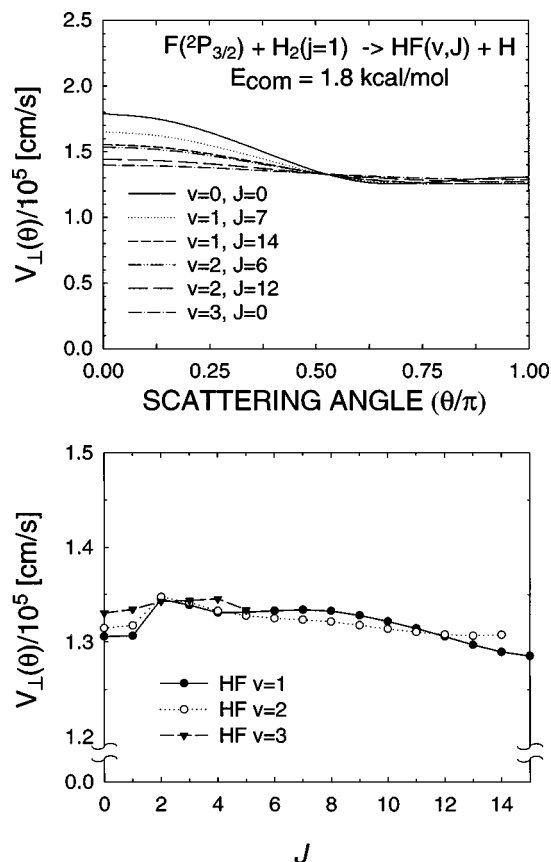

FIG. 11. Diagnostic tests of the density-to-flux transformation behavior for F+H$_2$ in the right angle crossed-jet collision geometry depends on the average final HF(v,j) velocity component perpendicular to the probe laser beam axis, which can be predicted from theoretical differential cross section calculations by Castillo and Manolopoulos.[58] Top: Perpendicular velocities as a function of center-of-mass scattering angle for a series of vibration/rotation levels. Bottom: Perpendicular velocities integrated over all center-of-mass scattering angles as a function of J for HF(v) in $v=1$, 2, and 3 manifolds. Note the remarkable insensitivity to HF(v,J) product state.

ferential and integral cross sections into given HF(v,J) levels on the ground-state adiabatic potential surface of Stark and Werner.[27] These differential cross sections can be related to the experimentally observed column-integrated populations by the standard center-of-mass to lab-frame transformation. As discussed above, however, the resulting flux-to-concentration transformation between integral cross sections and populations for the current scattering geometry, kinematic mass combinations and energetics is essentially independent of HF(v,J). Thus, we can directly compare the experimental column-integrated populations with the theoretical integral cross sections, averaged over the 1:3 nuclear spin distribution of $j=0$ (para) and $j=1$ (ortho) H$_2$

TABLE II. Nascent vibrational HF populations (summed over J).

V	Population (%)
0	<2(2)
1	18.8(32)
2	54.2(23)
3	27.0(5)

J. Chem. Phys., Vol. 109, No. 21, 1 December 1998

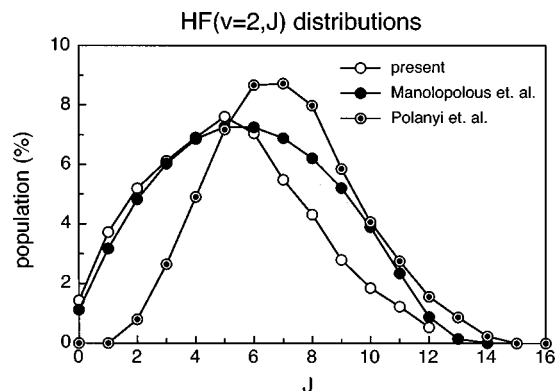Chapman *et al.*   9315

HF(v=2,J) distributions

FIG. 12. Comparison of the rotationally resolved HF($v=2,J$) product state distributions with (a) exact quantum close coupled theory[58] on the SW potential surface[27] and (b) arrested relaxation studies by Polanyi and Woodall.[4]

HF vibrational branching ratios

FIG. 13. Comparison of rotationally unresolved branching ratios into $v = 1$, 2, and 3 from (a) arrested relaxation studies of Polanyi and Woodall,[4] (b) crossed-molecular-beam studies of Neumark *et al.*,[34,35] (c) the current work, and (d) theoretical predictions by Castillo and Manolopoulos.[58]

in the low-temperature jet. These comparisons are displayed in Fig. 9, which shows measured and predicted product state distributions (in % of total) for $E_{com}=2.4(6)$ and 1.84 kcal/mole, respectively.

The data indicate several points worth noting. First of all, the qualitative overall trends in experimental rovibrational populations are in remarkably good agreement with exact quantum theoretical predictions by Castillo and Manolopoulos[28,58] on the Stark and Werner (SW) potential energy surface.[27] In the $v=2$ manifold, for example [Fig. 9(b)], both experiment and theory indicate a broad J-distribution rising from low J and peaking at $J=5$. The measured drop-off in population at higher J is slightly sharper than predicted theoretically, but the relative populations at $J=11$ and 12 are again comparable. The distribution of $v =1$ rotational states is broader still and reasonably well matched by theory [Fig. 9(c)]. The sharp peaking of the $v =3$ rotational distributions near $J\approx1-2$ is also well reproduced, although more significant deviations are clearly evident at higher J-values. Nevertheless, the overall level of agreement is impressive and indicates strong support both for the SW potential surface[27] as well as the quantum dynamical calculations of Castillo and Manolopoulos.[58]

Though the main thrust of this paper is to compare with quantum theoretical predictions, it is also worth briefly comparing with HF(v,J) populations observed in the early arrested relaxation studies of Polanyi and co-workers.[3–5] Since the HF($v=2$) rotational levels represent the majority of the reactive flux, this vibrational manifold is chosen for comparison in Fig. 12, where the Polanyi data reflects their best extrapolation to zero-pressure, fully "arrested" experimental conditions. Although the two sets of experimental results are qualitatively similar, significant differences are also clearly evident. Specifically, the crossed-jet distributions start at nonzero values at $J=0$ and grow to a maximum by $J=5$, whereas the arrested relaxation studies suggest vanishing $J =0$ and 1 populations that grow to a more symmetric maximum at $J=7$. This trend in the crossed-jet results toward lower J-state distributions might, at first, suggest partial rotational relaxation. However, this is quite unlikely, since the crossed-jet data are obtained for more than 2 orders of magnitude lower average pressures in the beam intersection re-
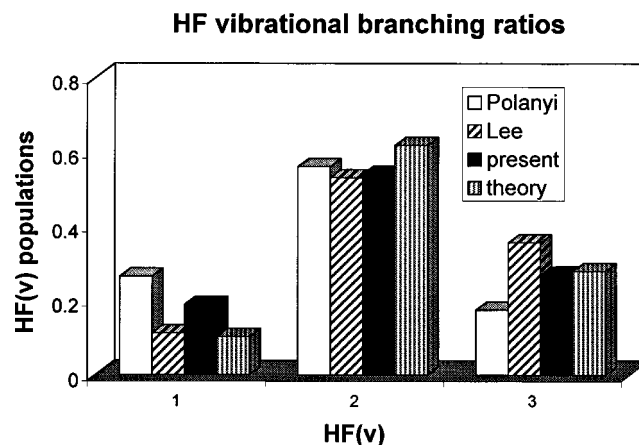
gion. Furthermore, the crossed-jet data are insensitive to a fourfold increase in this crossing density, as indicated in Fig. 10. This is qualitatively different from arrested relaxation studies, where the data required explicit correction for pressure-dependent effects. Finally, it is worth noting that the experimental distributions for $v=1$ and 2 appear less symmetric than theoretically predicted from quantum calculations by Castillo and Manolopoulos on the lowest adiabatic surface, which also differs from the more symmetric distributions for these two manifolds reported by Polanyi and Woodall.[4]

By summing over all rotational states in a given vibrational manifold, we can also include previous crossed-beam studies by Neumark *et al.*[34,35] in these comparisons. These vibrational branching ratios for all three experimental studies are presented in Fig. 13, and compared again with the theoretical predictions of Castillo *et al.*[28] on the SW lowest adiabatic potential energy surface.[27] First, the results indicate fairly good agreement between the present crossed-jet and previous crossed-beam studies. This is especially impressive since the two methods utilize fundamentally different detection schemes (i.e., IR absorption/emission vs electron bombardment ionization) for characterizing the product state vibrational distributions. Second, the overall agreement between experiments and theory is quite reasonable, although some significant differences can be noted. Specifically, theory predicts less population in $v=1$ by nearly twofold than is observed. This would suggest, despite the remarkably good agreement between theory and experiment for trends in the rotationally resolved quantum state distributions, that there still may be qualitatively important issues to be addressed in either the *ab initio* surfaces or the dynamics calculations.

In this regard, it is interesting to look more closely at discrepancies between theory and the current experimental results. These are most clearly evident in the $v=3$ manifold [Fig. 9(a)] for which calculations on the SW surface predict a significantly steeper decrease in population with increasing J than experimentally observed. Specifically, the fraction of

$v=3$ population measured in $J=3$ is nearly twofold larger than theoretically predicted, while this factor grows to nearly sixfold for $J=4$. This effect is even more dramatic in $J=5$, which is predicted to be an *energetically closed* channel on the Stark and Werner surface (i.e., the integral cross section vanishes identically), whereas strong experimental signals at $J=5$ are clearly evident. The source of this qualitative discrepancy can be easily traced to errors in the potential energy surface of SW.[27] Specifically, the dissociation energies of both H$_2$ ($D_0=36\,118.6(5)$ cm^{-1}) and HF ($D_0=47\,311(5)$ cm^{-1}) have been determined to high precision from detailed spectroscopic studies.[59,60] Thus, the corresponding overall reaction exothermicity for ground spin orbit excited F($^2P_{3/2}$) with para H$_2(j=0)$ is $\Delta E=11\,192(5)$ cm^{-1} [32.001(14) kcal/mole]. With ortho H$_2(j=1)$ reagent, this makes the HF($v=3,J=5$) product channel exothermic by $\approx 0.7(6)$ kcal/mole at the collision energies used in this work. By way of contrast, the Stark and Werner surface yields an overall reaction exothermicity of only $\Delta E=31.77$ kcals/mole, which is 0.23 kcals/mole *smaller* than experimentally determined, and is the reason why the theoretically predicted HF($v=3,J=5$) populations vanish identically at $E_{com}=1.84$ kcal/mole. These discrepancies underscore the necessity of improving the asymptotic exit/entrance channel properties of the SW surface in order to reliably predict quantum state-resolved reaction dynamics near the energetic threshold.

As a final note, closer inspection of Fig. 9 and Table I reveals that there is also some finite population observed in HF($v=3,J=6$). This state is at the energetic upper limit and thus essentially requires the full center-of-mass collision energy plus the reaction exothermicity to access, even for the limiting case of zero kinetic collision energy recoil in the products. Such product state behavior is more dramatic in studies at lower collision energies, which reveal HF($v=3,J$) population in several rotational levels *above* the energetically accessible limit for reactions of ground spin-orbit F($^2P_{3/2}$) with either para or ortho H$_2(j=0,1)$. It is worth noting, however, that these HF(v,J) product channels would be energetically accessible from spin-orbit-excited F*($^2P_{1/2}$) atoms at 1.15 kcal/mole higher energy, and also present in the supersonic discharge beam. This latter possibility is especially intriguing, since it would suggest contributions from *nonadiabatic* reaction pathways involving more than the lowest Born–Oppenheimer potential surface, a topic of considerable theoretical importance in the calculation of state-to-state reaction dynamics.[61–70] The possible role of such nonadiabatic processes, as elucidated by state-to-state cross section measurements as a function of center-of-mass collision energy, will be addressed elsewhere in detail.[57]

VII. SUMMARY

A new direct IR laser absorption-based method is described that permits nascent rotational and vibrational product distributions to be determined for F+H$_2$→HF+H reactions in crossed supersonic expansions under single collision conditions. Populations extracted from absorption and stimulated emission signals show very good overall agreement with the predictions of Castillo and Manolopoulos[28] on the

ground adiabatic potential energy surface of Stark and Werner,[27] over most of the HF(v,J) state distribution. Comparison with the early arrested relaxation studies of Polanyi and Woodall[4] indicates qualitatively good but somewhat less satisfactory agreement with both the present results as well as theoretical calculations, especially for rotational distributions in the maximally populated $v=2$ manifold. Summed over all rotational states, the current product state distributions are in reasonable agreement with previous vibrationally resolved crossed-beam measurements of Lee and co-workers[34,35] obtained under lower energy resolution conditions, as well as with the theoretical predictions of Castillo and Manolopoulos.[28,58]

In terms of nascent state populations, the present rovibrationally resolved results represent the most rigorous test of both *ab initio* and dynamics theory to date; the very favorable agreement indicates strong support for both the quality of the potential as well as the ability to perform accurate full quantum coupled calculations on a single adiabatic surface. At a more detailed level of inspection, however, there is clear evidence for outstanding discrepancies between theory and experiment that warrant further attention. Specifically, theory significantly *underpredicts* population in the highest energetically accessible rotational levels in the $v=3$ manifold states, by as much as factors of 5 or more. This point is most clearly made in the HF($v=3,J=5$) level, which is energetically closed on the Stark and Werner surface[27] at 1.84 kcal/mole, yet still energetically accessible from accurate thermochemical predictions and experimentally observed. This highlights the need for further refinement of the exit and entrance channels on the F+H$_2$ surface in order for such threshold phenomena to be reliably explored with fully rigorous quantum dynamics calculations.

[1] G. C. Schatz, J. Phys. Chem. **100**, 12839 (1996).

[2] D. E. Manolopoulos, J. Chem. Soc., Faraday Trans. **93**, 673 (1997).

[3] J. C. Polanyi and D. C. Tardy, J. Chem. Phys. **51**, 5717 (1969).

[4] J. C. Polanyi and K. B. Woodall, J. Chem. Phys. **57**, 1574 (1972); D. H. Maylotte, J. C. Polanyi, and K. B. Woodall, *ibid.* **57**, 1547 (1972).

[5] K. G. Anlauf, P. J. Kuntz, D. H. Maylotte, P. D. Pacey, and J. C. Polanyi, Discuss. Faraday Soc. **44**, 183 (1967).

[6] J. H. Parker and G. C. Pimentel, J. Chem. Phys. **51**, 91 (1969).

[7] T. P. Schafer, P. E. Siska, J. M. Parson, F. P. Tully, Y. C. Wong, and Y. T. Lee, J. Chem. Phys. **53**, 3385 (1970).

[8] C. F. Bender, P. K. Pearson, S. V. ONeil, and H. F. Schaefer III, J. Chem. Phys. **56**, 4626 (1972).

[9] J. T. Muckerman, J. Chem. Phys. **56**, 2997 (1972).

[10] R. Steckler, D. G. Truhlar, and B. C. Garrett, J. Chem. Phys. **82**, 5499 (1985).

[11] T. Takayanagi and S. Sato, Chem. Phys. Lett. **144**, 191 (1988).

[12] G. C. Lynch, R. Steckler, D. W. Schwenke, A. J. C. Varandas, and D. G. Truhlar, J. Chem. Phys. **94**, 7136 (1991).

[13] R. L. Jaffe, J. M. Henry, and J. B. Anderson, J. Chem. Phys. **59**, 1128 (1973).

[14] J. T. Muckerman, J. Chem. Phys. **57**, 3382 (1972).

[15] R. L. Wilkins, J. Chem. Phys. **57**, 912 (1972).

[16] A. Komornicki, T. F. George, and K. Morokuma, J. Chem. Phys. **65**, 4312 (1976).

[17] W. Jakubetz and J. N. L. Connor, Faraday Discuss. Chem. Soc. **62**, 324 (1977).

[18] D. Neuhauser, R. S. Judson, R. L. Jaffe, M. Baer, and D. J. Kouri, Chem. Phys. Lett. **176**, 546 (1991).

[19] F. J. Aoiz, L. Banares, V. J. Herrero, V. Saez Rabanos, K. Stark, and H.-J. Werner, J. Chem. Phys. **102**, 10665 (1994).

[20] G. C. Schatz, J. M. Bowman, and A. Kuppermann, J. Chem. Phys. **63**, 674 (1975).

[21] J. Z. H. Zhang and W. H. Miller, J. Chem. Phys. **88**, 4549 (1988).

[22] J. M. Launay and M. Le Dourneuf, Chem. Phys. Lett. **169**, 473 (1990).

[23] J. Z. H. Zhang, Chem. Phys. Lett. **181**, 63 (1991).

[24] E. Rosenman, S. Hochman-Kowal, A. Persky, and M. Baer, Chem. Phys. Lett. **239**, 141 (1995).

[25] G. D. Billing, L. Y. Rusin, and M. B. Sevryuk, J. Chem. Phys. **103**, 2482 (1995).

[26] D. E. Manolopoulos, K. Stark, H.-J. Werner, D. W. Arnold, S. E. Bradforth, and D. M. Neumark, Science **262**, (1993).

[27] K. Stark and H.-J. Werner, J. Chem. Phys. **104**, 6515 (1996).

[28] J. F. Castillo, D. E. Manolopoulos, K. Stark, and H.-J. Werner, J. Chem. Phys. **104**, 6531 (1996).

[29] P. D. Mercer and H. O. Pritchard, J. Phys. Chem. **65**, 1468 (1959).

[30] E. Wurzberg and P. L. Houston, J. Chem. Phys. **72**, 4811 (1980).

[31] R. F. I. Heidner, J. F. Bott, C. E. Gardner, and J. E. Melzer, J. Chem. Phys. **72**, 4815 (1980).

[32] J. H. Parker and G. C. Pimentel, J. Chem. Phys. **55**, 857 (1971).

[33] R. D. Coombe and G. C. Pimentel, J. Chem. Phys. **59**, 1535 (1973).

[34] D. M. Neumark, A. M. Wodtke, G. N. Robinson, C. C. Hayden, and Y. T. Lee, J. Chem. Phys. **82**, 3045 (1985).

[35] D. M. Neumark, A. M. Wodtke, G. N. Robinson, C. C. Hayden, K. Shobatake, R. K. Sparks, T. P. Schafer, and Y. T. Lee, J. Chem. Phys. **82**, 3067 (1985).

[36] M. Faubel, L. Y. Rusin, S. Schlemmer, F. Sondermann, U. Tappe, and J. P. Toennies, J. Chem. Soc., Faraday Trans. **89**, 1475 (1993).

[37] M. Faubel, L. Rusin, S. Schlemmer, F. Sondermann, U. Tappe, and J. P. Toennies, J. Chem. Phys. **101**, 2106 (1994).

[38] M. Faubel, Z. Phys. Chem. (Munich) **188**, 197 (1995).

[39] S. E. Bradforth, D. W. Arnold, D. M. Neumark, and D. E. Manolopoulos, J. Chem. Phys. **99**, 6345 (1993).

[40] A. Weaver, R. B. Metz, S. E. Bradforth, and D. M. Neumark, J. Chem. Phys. **93**, 5352 (1990).

[41] A. Weaver and D. M. Neumark, Faraday Discuss. Chem. Soc. **91**, 5 (1991).

[42] D. T. Anderson, S. Davis, T. Zwier, and D. J. Nesbitt, Chem. Phys. Lett. **258**, 207 (1996).

[43] S. Davis, D. T. Anderson, G. Duxbury, and D. J. Nesbitt, J. Chem. Phys. **107**, 5661 (1997).

[44] W. B. Chapman, B. W. Blackmon, and D. J. Nesbitt, J. Chem. Phys. **107**, 8193 (1997).

[45] G. Dharmasena, T. R. Phillips, K. N. Shokirev, G. A. Parker, and M. Keil, J. Chem. Phys. **106**, 9950 (1997).

[46] D. Smith and P. Spanel, Adv. At., Mol., Opt. Phys. **32**, 307 (1994).

[47] L. M. Branscomb, *Atomic and Molecular Processes*, edited by D. R. Bates (Academic, New York, 1962).

[48] D. Proch and T. Trickl, Rev. Sci. Instrum. **60**, 713 (1989).

[49] A. S. Pine, A. Fried and J. W. Elkins, J. Mol. Spectrosc. **109**, 30 (1985).

[50] D. Herriott, H. Kogelnik, and R. Kompfner, Appl. Opt. **3**, 523 (1964).

[51] R. S. Ram, Z. Morbi, B. Guo, K.-Q. Zhang, P. F. Bernath, J. Vander Auwera, J. W. C. Johns, and S. P. Davis, Astrophys. J., Suppl. Ser. **103**, 247 (1996).

[52] A. S. Pine, A. Fried, and J. W. Elkins, J. Mol. Spectrosc. **109**, 30 (1985).

[53] J. L. Hall and S. A. Lee, Appl. Phys. Lett. **29**, 367 (1976).

[54] E. Arunan, D. W. Setser, and J. F. Ogilvie, J. Chem. Phys. **97**, 1734 (1992).

[55] W. B. Chapman, M. J. Weida, and D. J. Nesbitt, J. Chem. Phys. **106**, 2248 (1997).

[56] G. Scoles, editor, *Atomic and Molecular Beam Methods*, Vol. I (Oxford University Press, New York, 1988).

[57] S. Nizkorodov, W. Harper, W. B. Chapman, B. W. Blackmon, and D. J. Nesbitt (unpublished).

[58] J. F. Castillo and D. Manolopoulos (private communication).

[59] W. C. Stwalley, Chem. Phys. Lett. **6**, 241 (1970).

[60] W. T. Zenke, W. C. Stwalley, J. A. Coxon, and P. G. Hajigeorgiou, Chem. Phys. Lett. **177**, 412 (1991).

[61] N. C. Blais and D. G. Truhlar, J. Chem. Phys. **58**, 1090 (1973).

[62] J. C. Tully, J. Chem. Phys. **60**, 3042 (1974).

[63] F. Rebentrost and W. A. Lester, Jr., J. Chem. Phys. **67**, 3367 (1977).

[64] I. H. Zimmerman, M. Baer, and T. F. George, J. Chem. Phys. **71**, 4132 (1979).

[65] M. B. Faist and J. T. Muckerman, J. Chem. Phys. **71**, 233 (1979).

[66] R. E. Wyatt and R. B. Walker, J. Chem. Phys. **70**, 1501 (1979).

[67] H.-D. Meyer and W. H. Miller, J. Chem. Phys. **71**, 2156 (1979).

[68] D. E. Fitz and D. J. Kouri, J. Chem. Phys. **74**, 3933 (1981).

[69] B. LePetit, J. M. Launay, and M. LeDourneuf, Chem. Phys. **106**, 111 (1986).

[70] M. Gilibert and M. Baer, J. Phys. Chem. **98**, 12822 (1994).